Neurobiology of Disease 129 (2019) 182–194

Contents lists available at ScienceDirect

Neurobiology of Disease

journal homepage: www.elsevier.com/locate/ynbdi

V232M substitution restricts a distinct O-glycosylation of PLD3 and its neuroprotective function

Atanas Vladimirov Demirev[a,1], Ha-Lim Song[b,c,1], Mi-Hyang Cho[b], Kwangmin Cho[c], Jong-Jin Peak[b], Hyun Ju Yoo[d], Dong-Hou Kim[b,*], Seung-Yong Yoon[b,c,*]

[a] Department of Microbiology, College of Medicine, Korea University, Seoul, Republic of Korea
[b] Department of Brain Science, Asan Medical Center, Bio-Medical Institute of Technology (BMIT), University of Ulsan College of Medicine, Seoul, Republic of Korea
[c] ADEL Institute of Science and Technology (AIST), ADEL, Inc., Seoul, Republic of Korea
[d] Department of Convergence Medicine, Asan Institute for Life Sciences, Asan Medical Center, University of Ulsan College of Medicine, Seoul, Republic of Korea

ARTICLE INFO

Keywords:
Phospholipase D3
Lipid metabolism
Alzheimer's disease
Memory impairment
Neurodegeneration
Val232Met
Lysosome

ABSTRACT

The link between Val232Met variant of phospholipase D3 (PLD3) and late-onset Alzheimer's disease (AD) is still obscure. While it may not affect directly the amyloid precursor protein function, PLD3 could be regulating multiple cellular compartments. Here, we investigated the function of wild-type human PLD3 ($PLD3^{WT}$) and the Val232Met variant ($PLD3^{VM}$) in the presence of β-amyloid (Aβ) in a *Drosophila melanogaster* model of AD. We expressed $PLD3^{WT}$ in CNS of the Aβ-model flies and monitored its effect on the ER stress, cell apoptosis and recovery the Aβ-induced cognitive impairment. The expression reduced ER stress and neuronal apoptosis, which resulted in normalized antioxidative phospholipids levels and brain protection. A specific O-glycosylation at pT271 in PLD3 is essential for its normal trafficking and cellular localization. The V232 M substitution impairs this O-glycosylation, leading to enlarged lysosomes and plausibly aberrant protein recycling. $PLD3^{VM}$ was less neuroprotective, and while, $PLD3^{WT}$ expression enhances the lysosomal functions, V232 M attenuated PLD3's trafficking to the lysosomes. Thus, the V232 M mutation may affect AD pathogenesis. Further understanding of the mechanistic role of PLD3 in AD could lead to developing novel therapeutic agents.

1. Introduction

Phospholipase D3 (PLD3), a type-II transmembrane protein of the PLD family, shows neuronal expression in the frontal and temporal cortices of human brains but does not colocalize with activated microglia or astrocytes (Hawrylycz et al., 2012; Lein et al., 2007; Munck et al., 2005; Satoh et al., 2014). Compared to PLD1, PLD2, and other genes that constitute a risk in developing Alzheimer's disease (AD) (Karch and Goate, 2015), the role of PLD3 in AD pathogenesis is still unclear. PLD1 corrects impaired trafficking of the amyloid precursor protein (APP) and negatively regulates γ-secretase activity to decrease β-amyloid (Aβ) levels (Cai et al., 2006a; Cai et al., 2006b). PLD2 associated with oligomeric Aβ-induced synaptic dysfunction (Oliveira et al., 2010). In AD brains, PLD3 protein levels are moderately decreased and transcription levels downregulated (Kong et al., 2009; Xu et al., 2006). PLD3 accumulates in cortical neuritic plaques (Satoh et al., 2014), raising the question of how it associates with AD pathology. PLD3 was reported to localize in secretory granules in a pancreatic β-cell line (Brunner et al., 2007) and partially overlapped with lysosomes in HeLa cells (Fazzari et al., 2017; Palmieri et al., 2011), suggesting involvement in trafficking through an endosome-lysosome pathway and a more complex function than robust endoplasmic reticulum (ER) homeostasis (Munck et al., 2005). In contrast to PLD1 and PLD2, the HKD motifs of PLD3 are in the luminal C-terminal domain (Fig. S1A and B) (Munck et al., 2005; Nelson and Frohman, 2015) and thus it could utilize lipids on the luminal side of the membrane or could have a key membrane function within other cellular compartments.

Cruchaga et al. first reported the rare PLD3 variant, Val232Met, as a risk factor for AD in a whole-exome sequencing set of late-onset AD (LOAD) coupled with genotyping from seven independent data sets comprised of 4998 Alzheimer's disease cases and 6356 controls of European descent (Cruchaga et al., 2014). They proposed that PLD3 is involved in amyloid precursor protein (APP) processing and that mutations in PLD3 such as pV232 M (hereafter referred to as $PLD3^{VM}$)

* Corresponding authors at: Alzheimer's Disease Experts Lab (ADEL), Department of Brain Science, University of Ulsan College of Medicine, 88, Olympic-ro 43-gil, SongPa-Gu, Seoul 05505, Republic of Korea.
E-mail addresses: yoohyunju@amc.seoul.kr (H.J. Yoo), dhkim@amc.seoul.kr (D.-H. Kim), ysy@amc.seoul.kr (S.-Y. Yoon).
[1] These authors contributed equally.

https://doi.org/10.1016/j.nbd.2019.05.015
Received 24 December 2018; Received in revised form 15 April 2019; Accepted 17 May 2019
Available online 20 May 2019
0969-9961/

could increase the Aβ levels. A later combined meta-analysis for the V232 M substitution also found an association of modest effect size in Han Chinese AD patients (Zhang et al., 2016). Zhang et al. supported the hypothesis proposed by Cruchaga et al. (Cruchaga et al., 2014) and speculated that the V232 M alters the 3D protein structure in an evolutionally conserved region located in proximity with the first HKD motif (Fig. S1). However, the search for rare PLD3 variants associated with an elevated risk for LOAD produced contrasting results. Three other independent groups failed to correlate the V232 M variant with AD in diverse European populations (Heilmann et al., 2015; Hooli et al., 2015; Lambert et al., 2015). Recently, Fazzari et al. (Fazzari et al., 2017) challenged the mechanistic model proposed by Cruchaga et al. (Cruchaga et al., 2014) and speculated that PLD3-knockout in mice did not affect APP processing. They provided an exciting finding that PLD3-knockout mice produced enlarged lysosomes instead of affecting APP processing, suggesting that PLD3 could be involved in lysosome regulation. Although they observed no apparent phenotype in the young ages of PLD3 knockout mice compared with wild-type mice, Fazzari et al. (Fazzari et al., 2017) did not show whether PLD3 knockout may produce degenerative phenotypes when associated with neurological conditions in the aged animals. Meanwhile, whether PLD3^{VM} is a contributing factor in LOAD pathogenesis is still unclear due to insufficient in vivo data.

Cross-species conservation allows employing *D. melanogaster* as a robust system for modeling human pathologies (Bier, 2005). Expression of β-amyloid-containing the Arctic mutation (Aβ42^{arc}) in *D. melanogaster* brain produces neurodegeneration with behavioral and cognitive deficits (Crowther et al., 2005). Thus, we could observe the effects of PLD3^{VM} expression on β-amyloid pathology in a model organism which normaly do not process APP and provide an APP-independent insights on the PLD3 cellular function. The closest homologues of PLD3 are found in other mammals (i.e. the murine SAM9 (Pedersen et al., 1998)) with ~93% identical amino acid residues (Fig. S1B) but more distantly related proteins as in *Xenopus* (54%) and *Drosophila* (44%) also constituted the very conserved HKD motifs (Munck et al., 2005). Our analysis (Fig. S1) revealed that human PLD3 share > 43% identical code with *D. melanogaster* ortholog and besides the HKD motifs, the two key positions discussed in this research, pV232 (reported also by (Zhang et al., 2016)) and pT271 are very conserved. Here, we present evidence that human wild-type (WT) PLD3 has a protective function in fruit fly brains against Aβ42^{arc} neurotoxicity. PLD3^{VM}, however, showed an impaired glycosylation pattern, inefficient cellular localization in vitro, and palusible restricted function causing atypical changes in cellular lipid composition and compromised neuronal protection. Shifts in essential cellular compartment markers showed that PLD3^{VM} also affects the cellular structures and thus pose an effect on late-onset AD pathology.

2. Materials and methods

2.1. DNA constructs, transgenes, and point mutations

Full-length human *PLD3* cDNA was amplified from HEK293 cells (with the addition of an N-terminal FLAG tag and a C-terminal *hemagglutinin, HA)* using Phusion Flash PCR Master Mix (F548) from Thermo Scientific. We inserted the resulting *flag::pld3-WT::HA* (*pld3*^{WT}) gene construct in pcDNA5 for mammalian cell expression and pUAS-attB for the generation of over-expressing transgenic fly lines. The primers utilized in this study are listed in the supplementary Table S1. We designed all primer sets by Primer3 with a melting temperature (Tm) of about 60 °C. A single-nucleotide (GTG > ATG, Val232Met) point mutation was generated in PLD3^{WT} using a standard site-directed mutagenesis protocol (Zheng et al., 2004) with a forward primer 5′-GGTCAAGGAGCTGGGCATGGTCATGTACAACTGC-3′ and reverse primer 5′- GCAGTTGTACATGACCATGCCCAGCTCCTTGACC-3′. We also generated five independent substitutions (serine to alanine or threonine to alanine) with the site-directed mutagenesis method at the four predicted O-glycosylation sites (Fig. S1 and Primers in Table S1). The resulting PLD3 gene constructs were digested by *Hin*dIII and BamHI (Table S1, hPLD3 cloning primers) and inserted in pcDNA5 for mammalian cell expression.

2.2. Transgenic fly stocks and maintenance

The transgenic flies were grown and maintained at 25 °C and 60% humidity on a 12-h light-dark cycle and a standard cornmeal medium (recipe by Bloomington Drosophila Stock Centre, BDSC, Bloomington, Indiana, USA). We obtained *D. melanogaster* transgenic fly lines *elav*^{c155}-*GAL4* (#25750), and *UAS-Aβ42-arctic* (33,774 and 33,773) from BDSC. BestGene Inc. (MA, USA) microinjected *UAS-PLD3*^{WT}- and *UAS-PLD3*^{V232M}-containing plasmids into *D. melanogaster* embryos inserting the PLD3-transgenes at the *attP* site in the *VIE260B* genetic background, which is a fly line used to generate the VDRC-KK collection (Dietzl et al., 2007). The commercial UAS-RNAi lines are generated by hairpin repeats of ~300 bp (VDRC) and it is well established to use the Dicer2 (*UAS-Dcr2*) in order to achieve a reliable expression of gene-specific RNAi hairpins in *D. melanogaster* via co-expression of UAS-Dcr2 (Dietzl et al., 2007; Zeng et al., 2015). The *mb247-Gal4* driver line was a kind gift from Thomas Riemensperger (Pech et al., 2013). We backcrossed all transgenic fly lines for at least five generations to a w^{1118} line (#60000, VRDC), which is a well-known fly control line.

2.3. Reagents and antibodies

2.3.1. Reagents

This research employed endoglycosidase H (Endo-H, Roche), O-glycosidase (O-Gly, NEB), peptide-N-glycosidase-F (PNGase-F, NEB), Brefeldin A (Sigma-Aldrich, B7651), and Lysotracker Red DND-99 (Invitrogen, L7528). All endoglycosidase and BFA treatments were performed according to manufacturer protocols, for 2 h at 37 °C. We used LysoTracker Red DND-99 as a lysosome marker (acidic compartments) according to the manufacturer's protocol for live cells and then immunochemically stained with appropriate antibodies (see cell immunocytochemistry). We purchased a mixture of 3 independent siRNA targeting non-coding regions in PLD3 pre-mRNA, generated from introns – 3, 6 and 7, from Thermo Fisher Scientific.

2.3.2. Antibodies

We employed rat anti-HA (Roche, clone 3F10), rabbit anti-Bcl2 (Santa Cruz, sc-492), rabbit anti-cleaved caspase-3 (Cell Signaling, #9661), rabbit anti-LAMP1 (Abcam, ab13523), rabbit anti-cathepsin B (Santa Cruz, sc-13,985), mouse anti-cathepsin D (Invitrogen, MA5–17236), and mouse anti-beta actin (Sigma, A5441).

2.4. XBP1 in vivo alternative splicing

We isolated total RNA from fly heads (2–3 μg, four independent samples) and subjected it to qRT-PCR (Supplement methods). We amplified 177 bp fragments of *D. melanogaster* XBP1 (spliced form, XBP1s) and 200 bp (XBP1u, unspliced) using the following primers: forward, 5′ ACAGCAGCACAACACCAGATGC 3′; and reverse 5′ CTTTCCAGAGTGA GGCCAGGCT 3′. PCR conditions were: denaturation at 97 °C for 2 min, 35 cycles of 96 °C (10 s each), 58 °C for 10 s, 68 °C for 10 s, and 72 °C for 1 min. We separated the PCR products at 20 V/cm^2 on non-denaturing 5% polyacrylamide gels prepared in 1 × Tris-borate-EDTA buffer. DNA bands were visualized using GelRed (Biotium).

2.5. High-content imaging

Cells transfected with PLD3-HA constructs (WT, V232 M, and T271A) were trans-seeded into a 96-well black plate (Greiner Bio-One). Cells were incubated with LysoTracker Red DND-99 for 30 min at 37 °C

under 5% CO_2. After washing 2× in phosphate-buffered saline (PBS), the cells were fixed in 4% paraformaldehyde and labeled with HA antibody. For data acquisition, at least 8 images were acquired per well using automated confocal microscopy (Opera high-content system; Perkin-Elmer) and analyzed for Lysotracker size (Harmony and acapella software; Perkin-Elmer). On average, we analyzed approximately 6000 cells for each experimental condition.

2.6. Iodixanol-gradient fractionation

We harvested 50–200 mg HeLa-cell pellets containing PLD3 constructs (WT, V232 M, T271A, or mock-HA) in a 2 mL microcentrifuge tube at about 850 ×g for 2 min. By the manufacturer's instructions, the pellet was incubated in 800 μL of gradient fractionation solution A (89,839; Thermo Fisher Scientific) with protease inhibitor at −4 °C for 2 min. We added 800 μL of gradient fractionation solution B to the cell suspension on ice and the tube inverted several times to mix. We centrifuged the suspension at 500 ×*g* for 10 min at 4 °C. The resulting supernatant containing total protein and 15% iodixanol in 1600 μL was overlaid on top of an iodixanol density gradient, prepared according to the manufacturer's instructions (OptiPrep, Thermo Scientific). Gradients were composed of 800 μL of 30% iodixanol, 800 μL of 27%, 400 μL of 23%, 800 μL of 20%, and 400 μL of 17% (total 2 mL). Gradients were centrifuged at 145,000 ×*g* for 2 h at 4 °C. We collected fourteen 320-μL fractions from the top of the gradient, and we assessed the distributions of LAMP1 by western blot.

2.7. Co-immunoprecipitation

We treated human neuroblastoma cell line (SH-SY5Y cells) expressing HA-tagged PLD^{WT}, $PLD3^{V232M}$, or $PLD3^{T271A}$ with oligomeric $A\beta_{1–42}$ (1 μM) (see below). We lysed the cells in Lysis Buffer (Calbiochem; 1% digitonin, 50 mM HEPES, 100 mM NaCl, 10 mM $CaCl_2$ and 5 mM $MgCl_2$ at pH 7.6, supplemented with protease inhibitor cocktail (Sigma)) for 30 min at 4 °C. Lysates were precleared with Protein G Sepharose (GE Healthcare) for 1 h at 4 °C. We performed immunoprecipitation by overnight incubation with the anti-HA antibody (Roche) at 4 °C. Immune complexes were purified using Protein G Sepharose followed by three washes with 0.1% digitonin. We eluted immunoprecipitated proteins by boiling in sodium dodecyl sulfate (SDS) sample buffer. We assessed the immunoprecipitated samples or samples representing 5% of the input lysates by western blot.

2.8. Oligomerization of β-amyloid

Commercially available $A\beta_{1–42}$ (BACHEM, 0.5 mg) was dissolved in DMSO (1 mM) and aliquots stored at −80 °C. We used polypropylene microcentrifuge tubes with a reduced-binding (1.5 ml) for the aliquots and dilutions. We diluted 1 mM $A\beta_{1–42}$/DMSO aliquot with ice-cold, sterile 1× PBS, vortexed for 60 s and then incubated for 10–12 h at 4 °C. The resulting oligomeric $A\beta_{1–42}$ (500 μM) was vortexed and diluted to 1 μM (final 0.1% DMSO) in complete cell culture media (DMEM, supplemented with 10% Fetal Bovine Serum (FBS) and warmed to 37 °C before it was added to the cells. Complete culture media containing 0.1% DMSO was used as the control conditions.

2.9. Phospholipid sample preparation and quantification

We collected approximately 250 fly heads from *elav*^{c155}-*Gal4* > *Aβ42*^{arc} flies expressing PLD3 variants after 20 d after eclosion at 25 °C. Bulk lipids from three independent experimental samples per genotype were rapidly extracted using methanol (80% *v*/v) according to a protocol for metabolites analysis from *D. melanogaster* (Tennessen et al., 2014). The cuticle and cellular debris were removed by centrifugation at 14,000 rpm for 10 min at 4 °C. The supernatants were re-extracted with chloroform and samples centrifugated at 2000 ×*g* for 15 min. The organic phase was carefully collected, vacuum dried, and stored at −80 °C pending analysis by LC-MS/MS. We normalized the lipid extracts against the sample protein concentration before LC-MS/MS analysis. To further compensate for possible lipid loss during sample preparation before lipid extraction, phosphatidylethanolamine (PE) 16:0 D31–18:1 and phosphatidylcholine (PC) 18:0 D70–18:0 were added as internal standard (IS). The stable isotope-labeled IS normalize the samples, provide quality control, and allow for the monitoring of instrument efficiency (Tennessen et al., 2014). Additionally, negative controls that contain no fly tissue were prepared to detect chemical contamination and false-positive peaks during the subsequent LC-MS/MS analysis. The fold change vs. mock control was calculated for every unique phospholipid molecule, then the averaged phospholipid value was estimated for four general lipid groups. The phospholipid derivatives detected by LC-MS/MS were the C18 plasmalogens phosphatidylcholine (PC) [LPC, 18:1, 22:6, 20:4] and phosphatidylethanolamine (PE) [LPE, 18:1, 22:6, 20:4], plus total PC, total PE, and total diacylglycerols (DAG).

2.10. D. melanogaster tissue preparation, immunohistochemistry, and imaging

Whole, adult fly brains were dissected in 0.1 M phosphate buffer at pH 7.2 and fixed for 90 min in 4% paraformaldehyde in 1× phosphate-buffered saline (PBS) at pH 7.4 and 25 °C. The brains were washed 3× for 10 min in P/T (0.3% Triton X-100 in 1× PBS at pH 7.4) and stored in P/T overnight at 4 °C. After blocking for 2 h in 5% normal goat serum in P/T, the fly brains were immunolabeled overnight with mouse anti-Fas-II (1D4, DSHB) at 4 °C with very slow shaking. After three 20-min washes in P/T on the shaker, the tissue samples were incubated overnight with secondary antibodies at 4 °C, washed 3 × for 30 min at room temperature (RT) in P/T, equilibrated in Vectashield mounting solution (Vectashield, +DAPI) and mounted on glass slides.

2.11. Cell culture, plasmid transfection, and western blot analysis

We transfected human neuroblastoma (SH-SY5Y) and HeLa cells with PLD3-containing pcDNA5 plasmids using Lipofectamine 2000 (Invitrogen, #11668–019) according to the manufacturer's guidelines. After a 48-h incubation, we lysed the cells in lysis buffer (50 mM Tris-HCl, 250 mM NaCl, 0.1% NP-40, 1% Triton X-100, and 10% glycerol at pH 7.3) containing a phosphatase and protease inhibitor mix (Sigma). We incubated the cells in fresh media containing 1.0 μM oligomeric Aβ for 24 h. Extracts were centrifuged at 13,000 rpm for 10 min at 4 °C, and the levels of soluble protein were quantified using the Coomassie Plus-200 protein assay reagent (Pierce). We separated the protein extracts by SDS-PAGE and performed Western blots according to general methods. Images were analyzed using Image J (IJ 1.45 m) and organized in Illustrator CS6.

2.12. D. melanogaster survival assay

elav^{c155}*-Gal4* virgins were collected, sorted into batches of 50–100 flies, and crossed with age-matched males to produce the desired genotypes. We collected at least 120 male flies per genotype (expressing one copy of *Arctic Aβ*$_{1–42}$ and the *UAS* control) at d 0–1 after eclosion and aged on standard cornmeal food (Bloomington recipe) complemented with 1.5% agar. Each vial was 9.5 × 2.4 cm and was kept on its side at 25 °C and 60% humidity under a 12-h light-dark cycle. To avoid any mortality unrelated to phenotype, we optimized the sample size per vial to 23–25. We exchanged with fresh standard fly food every 2–3 days and counted the dead Aβ-flies. Differences in survival were analyzed using the Kaplan-Meier equation in GraphPad Prism 5 (GraphPad Software, Inc., La Jolla, CA).

2.13. Negative geotaxis assay

We assessed the climbing behavior of 120 male flies (23–25 per genotype) collected 0–1 d after eclosion in a clean 15-cm-high × 2.4-cm-diameter polystyrene vial. We transferred each genotype without anesthesia, give them 30–60 s of rest before and between trials, and gently tapped them to the vial bottom in a dark room under a red light (Paterson Safelight Photax Filter, SH2013011, UK). The data represent mean ± standard errors of the mean (SEM) of 6 independent experimental fly cohorts tested serially every 5 d within 50 d from d 0–1 after eclosion. We calculated the climbing activity by counting the number of flies above a mark on the vial at 2.5 cm, 15 s after tapping the vial and expressed the value as a percentage of the number of flies in the vial. Images (videos) were taken using a Sony DSC-90 Cyber-shot 8.1 camera placed and leveled 40 cm in front of the test vial.

2.14. Learning and memory assay

We used the two-choice, conditioned preference test for an odor associated or not associated with ethanol and performed a Y-maze assay, as described by Kaun et al. (Kaun et al., 2011). Specifically, we collected 8 to 16 groups of 10–12 male flies per genotype at 0–1 d after eclosion, incubated them at 25 °C and 50% humidity, and tested them at 20 d after eclosion. We trained the flies in a 15 × 15 × 15 cm chamber. Humidified air was simultaneously streamed through diluted odors at a flow rate of 1.0 $L{\cdot}min^{-1}$ and mixed with the ethanol vapor at 1.5 $L{\cdot}min^{-1}$ (resulting in 53% ethanol, *v*/v) in the training chamber at 23–24 °C to entrain alcohol vapor. We used a 2:1 mixture of ethyl acetate (1:50) and acetic acid (1:500) as odor A and isoamyl alcohol (1:50) as odor B. We diluted odorants in mineral oil and prepared ethanol before each training and testing sessions. Each training consisted of three repetitions spaced by 50–60 min of a 10-min exposure to odor A, a 5-min humidified air, and a 10-min odor B plus ethanol. A reciprocal group of flies was simultaneously trained using a 10-min odor B exposure, a 5–10 min exposure to humidified air, and a 10-min exposure to odor A plus ethanol. We assessed fly memory 30 min, and 24 h post-training and we give the flies 5 min to choose between odorant A or B.

We used a balanced procedure, to ensure that the subjective preferences for either odor did not affect conditioning. Testing flies with rapid neurodegeneration also had several confounds. We observed that, compared with control *elav*^{c155}*-Gal4/attP* flies, the *elav*^{c155}*-Gal4 > Aβ42*^{arc} flies more easily became intoxicated by the ethanol vapors and exhibited a high mortality rate. We noticed that age-dependent neurodegeneration in *elav*^{c155}*-Gal4 > Aβ42*^{arc} flies also causes their climbing abilities to decline rapidly at > 30 d after eclosion. After testing several assay conditions with *elav*^{c155}*-Gal4 > Aβ42*^{arc} flies, we concluded that at about 20 d after eclosion at 25 °C, Aβ-flies are still very active in the presence of 50% ethanol and the mortality rate is < 10% after the training. Therefore, we used Aβ-flies not older than 25 d after eclosion and alcohol concentration to 50–53% (*v*/v) which did not affect the memory performance of the WT flies (Fig. S3). Although well sedated after a 10-min exposure, Aβ-flies recover completely within 50 min postconditioning. Twenty to twenty-five days old *Aβ42*^{arc} flies show signs of neurodegeneration (Fig. 1B) but still exhibit a climbing activity of over 60%. All of the tested 20–25 d old *Aβ42*^{arc} fly genotypes exhibited equal preference when tested odor A vs. odor B in the absence of conditioning (Fig. S3), and therefore have a standard odorant-dependent attractive behavior. Aβ-flies also show a typical attractive behavior in the Y-maze when given 5 min to select between an unconditioned odor vs. air (Fig. S3B).

2.14.1. Data assessment

First, we calculated the preference index (PI) for the odor paired with ethanol (conditioned stimulus, CS) as PI = (the number of flies in the paired-odor arm – the number of flies in the unpaired-odor arm) / (total number of flies). Then we calculated a conditional preference index (CPI) for conditioned odor preference or aversion by averaging the preference indices for reciprocally trained groups of flies. Odor controls were performed as described above, except that instead of choosing between two different odors, flies chose between each of the odor A (B) versus air streamed through mineral oil. We calculated the PI as (number of flies in the odor arm – the number of flies in the air arm)/ (total number of flies).

2.15. D. melanogaster rough-eye phenotype

We collected *gmr-Gal4* transgenic virgins and crossed them to *UAS-Aβ42*^{arc}*, UAS-PLD3* male flies. We incubated up to 50 age-matched larvae (3–5 days post egg-laying) from each genotype in standard cornmeal food at 28 °C. Then we collected adult male flies 5–10 d after eclosion and assessed the presence of the rough-eye phenotype under a light stereomicroscope (5MP camera).

2.16. Quantitative PCR

We cut off heads of 30 animals (15 d after eclosion) using sharpened high precision tweezers and flash frozen in Eppendorf tubes on dry ice and stored in a dry state at −80 °C pending first-strand cDNA synthesis. For each experiment, We prepared six independent total RNA samples from frozen *D. melanogaster* heads with the desired genotype and control flies using TriZol (Sigma). For each sample, 3 μg total RNA (NanoDrop) was reverse transcribed using a cDNA synthesis kit (SuperScript® III, Thermo Fisher, #18080051). Gene expression levels were assayed in 96-well plates using a BioRad SYBRGreen kit according to the manufacturer's protocol.

2.17. Flow cytometry

We transfected 1 × 10^5 HeLa cells with the PLD3-HA constructs WT, V232 M, and T271A, and Mock (Control). After washing with PBS, cells were detached and re-suspended in PBS with 0.125% Trypsin-EDTA. HA-antibody was then added and incubated at 4 °C for 30 min. Then washed cells were incubated at 4 °C for 30 min with 1 μg/mL of Alexa Fluor 488 anti-rat IgG antibody (Invitrogen). Finally, the cells were resuspended and fixed in 500 μL of PBS containing 4% paraformaldehyde. At least 10,000 events were acquired and analyzed using the FACSCanto II flow cytometer (BD Bioscience, San Jose, CA, USA).

2.18. Cell immunocytochemistry

Cells on coverslips were fixed in 4% paraformaldehyde for 30 min at RT. Cells were washed thrice with 1× PBS, pH 7.4 and permeabilized with blocking buffer (1% Triton X-100, 5% goat serum, 1% bovine serum albumin (BSA) in PBS) for 30 min at RT. We incubated the cells with primary antibodies in a staining buffer (5% goat serum, 1% BSA in PBS) overnight at 4 °C. The next day, the cells were washed 6× for 5 min with PBS and then incubated with secondary antibodies in staining buffer for 1 h at RT. Then we washed 6× for 5 min with PBS, and we stained the cells with Hoechst for 5 min. After washing 3× for 5 min with PBS, we mounted the coverslips on glass slides with mounting medium (Dako). All digital images were acquired using a Nikon microscope and were filtered and processed using NIS software.

2.19. Statistical analyses

We performed statistical analysis by One-Way ANOVA followed by Bonferroni's post-hoc comparison test, **, P < .01. Mean survival time comparisons for *Aβ42*^{arc} flies were performed using the Mantel-Cox test. Values are presented as means ± SEM of at least three independent experiments.

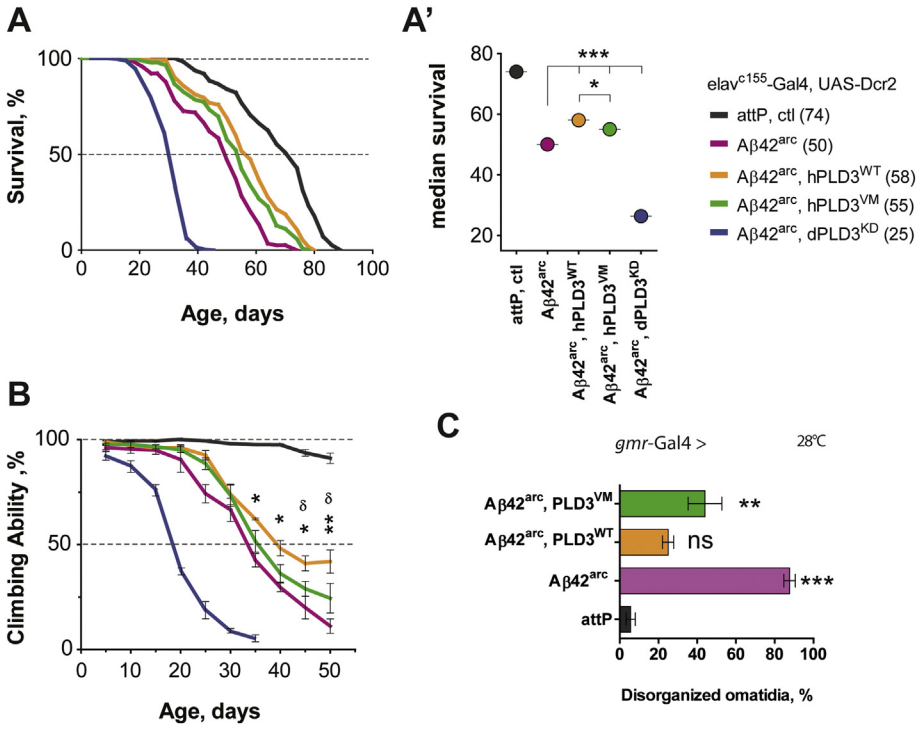

Fig. 1. Phospholipase D3 (PLD3^{WT}) is protective against behavioral and developmental effects of Aβ accumulation in a fly model of AD, V232 M variant (PLD3^{VM}) less so.

Longevity (A) and age-dependent decline of negative geotaxis (B) of Aβ42^{arc} flies expressing PLD3 wild-type (WT) (PLD3^{WT}), PLD3-V232 M variant (PLD3^{VM}), or PLD3-RNAi (dPLD3^{KD}). We compared all genotypes to the control flies (with *attP* or *Aβ42^{arc}*). The climbing ability (B) and median survival (A') of *Aβ42^{arc}, PLD3^{WT}* flies are significantly improved compared with *Aβ42^{arc}, PLD3^{VM}* flies. The data points in (B) represent the mean ± standard error of the mean (SEM) of the percentage of flies able to climb above a 2.5-cm–high mark; n > 120 flies per genotype in (A) and (B). *, Aβ42^{arc}, PLD3^{WT} vs. Aβ42^{arc}; $^{\delta}$, Aβ42^{arc}, PLD3^{VM} vs. Aβ42^{arc}, PLD3^{WT}; *, P < 0.05; **, P < 0.01; $^{\delta}$, P < 0.05, One-Way ANOVA with Bonferroni's correction. All fly genotypes in (A) and (B) are under the control of the *elav^{c155}-Gal4* driver. (A') Comparisons of the mean survival times in (A) of each genotype is given in parentheses; ***, P < 0.001; *, P < 0.05; Mantel-Cox, GraphPad Prism. (C) The graph represents the fused ommatidia count. We analyzed the light stereomicrographs of fused ommatidia and rough-eye phenotypes in transgenic flies co-expressing Aβ42^{arc} and PLD3^{WT} or Aβ42^{arc} and the PLD3^{VM} mutant or Aβ42^{arc} and dPLD3^{KD} under the *gmr-Gal4* driver. n > 15 males per genotype. See also Fig. S2.

3. Results

3.1. Phospholipase D3 (PLD3^{WT}) is protective against behavioral and developmental effects of Aβ accumulation in a fly model of AD, V232 M variant (PLD3^{VM}) less so

First, we investigated the behavioral effects of two PLD3 variants on Aβ-induced neurotoxicity in the *D. melanogaster* central nervous system (CNS). We generated UAS-PLD3^{WT} and UAS-PLD3^{VM} transgenic flies and expressed the two PLD3 variants by the *elav^{c155}-Gal4* driver (Lin and Goodman, 1994). In order to achieve a reliable expression of gene-specific RNAi hairpins by *elav^{c155}-Gal4* driver in *D. melanogaster*, we co-expressed Dicer2 (*UAS-Dcr2,* hereafter *Dcr2*) (Dietzl et al., 2007; Zeng et al., 2015). The lifespan of flies expressing single copies of PLD3^{WT} or PLD3^{VM} by *elav^{c155}-Gal4* was not significantly different from that of the control flies, *elav^{c155}-Gal4, Dcr2 > attP* (Fig. S2A), implying no or low heterologous protein toxicity. Pan-neuronal expression of β-amyloid-containing the Arctic mutation (Aβ42^{arc}) in *D. melanogaster* (hereafter, "Aβ flies"), results in depletion of presynaptic axonal mitochondria as well as a presynaptic and postsynaptic loss (Crowther et al., 2005; Lin et al., 2014; Zhao et al., 2010). We observed that at 25 °C and 50% humidity, Aβ-flies exhibit markedly impaired motor activity and decreased lifespan (Fig. 1A). Interestingly, neuronal expression of PLD3^{WT} extends the Aβ flies' survival (median survival 58 d after eclosion vs. control Aβ flies, median survival 50 d; by the Mantel-Cox test). Although overexpression of the PLD3^{VM} also improves the Aβ flies' survival (median 55), these flies' lifespan was significantly shorter than that of the *elav^{c155}-Gal4, Dcr2 > Aβ42^{arc}, pld3^{WT}* flies (Fig. 1A and A'). Knockdown of *Drosophila* PLD3 (dPLD3^{KD}) reduces the endogenous transcription levels by 60%, which appears to be sufficient to deteriorate further the Aβ flies lifespan (Fig. 1A). To obtain stable and consistent expression of Aβ^{arc} peptide and PLD3 recombinant proteins, and reduce the false results, we incubated all fly genotypes at 25 °C and 50% humidity (Fig. S2B and S2C). Both ectopically expressed human PLD3 transgenes had similar transcription levels in the presence of a single copy of *elav^{c155}-Gal4* driver (Fig. S2B). Since the amyloid beta mRNA levels also exhibited similar levels at these conditions in all genotypes (5 d after eclosion), we concluded that the behavioral effects are dependent on PLD3 variants expression, without a promoter competition in this ectopic expression system, (Fig. S2C). All genotypes contained a single copy of *elav^{c155}-Gal4,* and *UAS-Dcr2* transgenes on the X-chromosome (Methods).

Next we observed how the expression of PLD3 variants can affect a neurodegenerative phenotype of Aβ flies. At 25 °C, Aβ-flies (*elav^{c155}-Gal4, Dcr2 > Aβ42^{arc}*) exhibit an age-dependent decline in their motor abilities starting about 10–15 d after eclosion that quickly deteriorates within 50 days (Fig. 1B). Consistent with the results from the survival assay, overexpression of PLD3^{WT} improved Aβ-flies climbing abilities. PLD3^{VM} was again less effective and compared with the control Aβ-flies (Fig. 1B). Knockdown of dPLD3 aggravates the Aβ-fly phenotype, further reducing survival (Fig. 1A) and climbing abilities (Fig. 1B). Expression of Aβ in the *D. melanogaster* eye by the glass multiple reporter promoter (Freeman, 1996; Ollmann et al., 2000) produces a rough-eye phenotype with asymmetric-fused ommatidia (*gmr-Gal4 > Aβ42^{arc}*), a developmental effect of Aβ accumulation observed in *D. melanogaster* compound eye (Fig. S2D). We counted the fused ommatidia and found that PLD3^{WT} expression significantly improved the degenerative phenotype while PLD3^{VM} expression was less efficient (Fig. 1C). PLD3^{VM} also slowed down Aβ-induced developmental defects, but it was less effective than PLD3^{WT} because we were able to see more disorganized and scrambled ommatidia (Fig. S2D). In conclusion, CNS expression of PLD3^{WT} is protective and can extend lifespan and improve the Aβ-flies motor abilities, while PLD3^{VM} shows a weaker protective effect, plausibly due to impaired function and or protein instability.

3.2. Ethanol-induced memory and neuronal plasticity in Aβ42arc flies are ameliorated only in the presence of PLD3^{WT}

Next, we asked whether Aβ induces cognitive impairment in Aβ-flies and whether PLD3^{WT} or PLD3^{VM} expression affects such impaired cognition. We assessed the cognitive performance in Aβ-flies by Y-maze, an ethanol-conditioned olfactory memory assay developed by Kaun et al. (Kaun et al., 2011) at 20–25 d after eclosion (Fig. 2A). All tested genotypes (under the *elav^{c155}-Gal4* driver (Lin and Goodman,

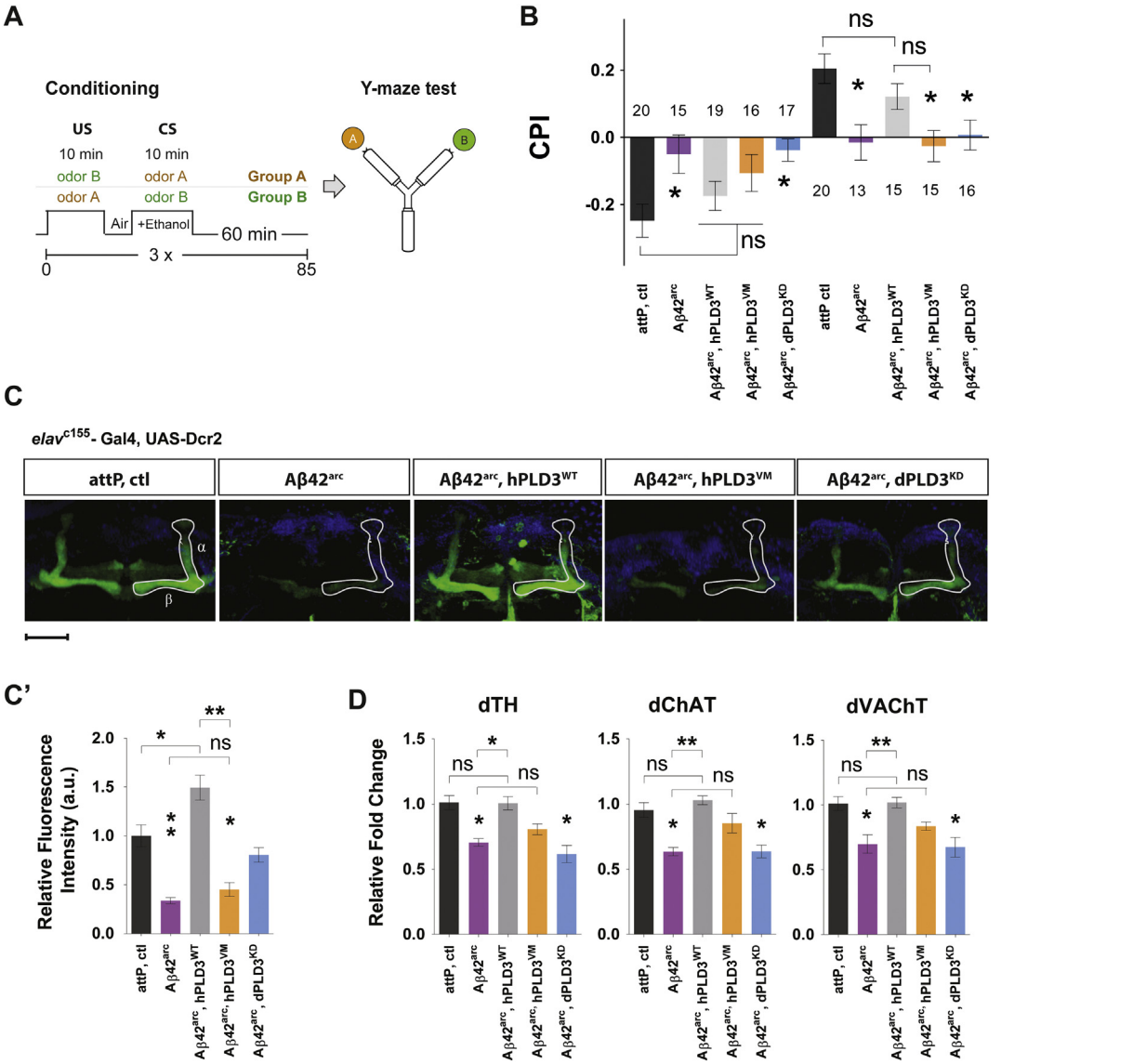

Fig. 2. Ethanol-induced memory and neuronal plasticity in *Aβ42^{arc}* flies are ameliorated only in the presence of PLD3^{WT}.
(A) We subjected Aβ-flies to three spaced training sessions of a 10-min exposure to a first odor (odor A) followed by a 5-min exposure to humidified air and a 10-min exposure to a second odor (odor B) paired with 40% ethanol vapor. The flies then choose between the two arms of a Y-maze containing different odors (odor A or odor B). (B) alcohol-conditioned aversion (30 min after training, short-term memory, STM) or preference (24 h after training, long-term memory, LTM) compared between flies expressing Aβ42^{arc} and PLD3^{WT}, Aβ42^{arc} and PLD3^{VM}, Aβ42^{arc} and dPLD3^{KD}, Aβ42^{arc} and attP, or control flies (n = 13–20 groups; each containing 10–12 flies/vial). Only Aβ42^{arc}, PLD3^{WT} flies show significant recovery of STM and LTM compared with the control and the other Aβ42^{arc} genotypes. (C) αβ neuron axonal projections in the mushroom bodies (MB) (αβ-MB lobes, top left, ctl) visualized in whole-mount, male brains (25–30 d after eclosion), stained for anti-Fascilin II (Fas-II, 1D4). We examined Fas-II signal intensity and compared the resulting image to the image of *elav^{c155}-Gal4/attP* control brains under blind-experiment with the same confocal acquisition settings. We observed reduced immunofluorescent intensity in the αβ-MB lobe of Aβ42^{arc} and Aβ42^{arc}, PLD3^{VM} flies but enhanced FasII signal in Aβ42^{arc}, PLD3^{WT} flies. (C′) graphical representation of the relative fluorescence intensity (FasII) of a designated area encompassing only the αβ-MB lobes (attP, CTL) represented in arbitrary units versus the control brains. (D) Quantitative RT-PCR analysis of dTH, tyrosine hydroxylase; dChAT, choline acetyltransferase; and dVAChT, vesicular acetylcholine transporter, from four independent total RNA samples derived from each specific genotype. All fly genotypes are under control of the *elav^{c155}-Gal4* driver (including *UAS-Dcr2*). CPI, conditional preference index; CS, conditioned stimulus; US, unconditioned stimulus. All data values are as mean ± SEM. *, P < 0.05; **, P < 0.01; One-Way ANOVA with Bonferroni's correction. Scale bar: 50 μm. See also Figs. S2, S3, and S4.

1994)) exhibited normal climbing abilities and odor preferences when control-tested with odor A (B) vs. air and no preference when control-tested with odor A vs. odor B (Fig. S3), implying an equally attractive olfactory behavior. The short-term ethanol-aversive memory (STM), assessed 30–60 min after training, and the long-term, ethanol-reward memory (LTM), tested 24 h after training, were significantly impaired in Aβ-flies (Fig. 2B). CNS expression of PLD3^{WT} in Aβ-flies resulted in the recovery of both aversive and reward memories (Fig. 2B), while PLD3^{VM} overexpression was unable to rescue impaired LTM-reward memory in Aβ-flies (Fig. 2B). Although statistically insignificant, we found a trend for the aversive memory deficit in PLD3^{VM}-expressing Aβ-flies vs. the attP control flies. A *mb247-Gal4* predominantly facilitate ectopic expression in Kenyon Cells (Pech et al., 2013) with projections into the mushroom bodies (MBs) (Davis and Han, 1996) a conserved, paired fly brain structure involved in fly memory processing that receives inputs from several sensory systems including the olfactory. Notably, we observed similar cognitive performances with the same genotypes expressed under *mb247-Gal4* driver (Fig. S4), where only PLD3^{WT} was advantageous and enhanced cognitive abilities, and PLD3^{VM} was not as effective.

Some neuronal cell-adhesion molecules such as *D. melanogaster* Fasciclin II (FasII), function as synapse stabilizing and destabilizing factors (Packard et al., 2003), and serves as a marker of the MBs αβ and γ lobes (Crittenden et al., 1998). We asked whether PLD3 variants expression, under the control of the *elav^{c155}-Gal4* driver, can improve synaptic stability in Aβ-fly brains. We stained whole brains from 25 to 30-d-old, male Aβ-flies with Fas-II (1D4) antibody (Fig. 2C) and found a decreased Fas-II intensity throughout the αβ and γ lobes of the MBs compared with brains from control flies (Fig. 2C, Left). In the same experimental conditions, we found that the αβ and γ lobes recovered in PLD3^{WT}-expressing Aβ flies. However, a decrease in FasII intensity was still observed after expression of PLD3^{VM} and to a lesser degree with dPLD3^{KD}. These data confirmed that neuronal rescue and synaptic stability is achieved only by PLD3^{WT} activity rather than by PLD^{VM} overexpression. Furthermore, the transcription levels of tyrosine hydroxylase, choline acetyltransferase (dChAT), and vesicular acetylcholine transporter (dVAChT) were significantly reduced in Aβ-fly heads (Fig. 2D), which may reflect the degeneration and recovery of dopaminergic and cholinergic neurons. Normal transcription levels were achieved only following PLD3^{WT} expression in Aβ flies.

3.3. PLD^{WT} rather PLD3^{VM} reduces Aβ-induced ER stress and neuronal apoptosis

Aβ activates alternative splicing of the X-box binding protein (XBP1) in vivo in a *D. melanogaster* AD model, as well as in mammalian neuron cultures (Casas-Tinto et al., 2011). The resulting ER stress produces a highly active transcription factor called XBP1s that targets the unfolded protein response (Yoshida et al., 2001). Four independent mRNA extracts showed that the active isoform of XBP1s is consistently increased in Aβ-fly brains (all genotypes were under *elav^{c155}-Gal4* driver) (Fig. 3A). We found that only the expression of PLD3^{WT} ameliorates the Aβ–induced ER stress in Aβ-flies at age 20–25 d after eclosion as indicated by lower levels of XBP1s. However, PLD3^{VM} or dPLD3^{KD} overexpression in Aβ-flies did not change XBP1s level significantly compared with control Aβ flies.

Bcl-2, an anti-apoptotic marker (Hockenbery, 1995), is also reduced in Aβ fly brain extracts, while cleaved caspase-3, an apoptotic cell death marker (Porter and Janicke, 1999), is increased (Fig. 3B). Bcl-2 localizes within the mitochondria and regulates Ca^{2+} release from the ER (Ferreiro et al., 2007). Increased expression of Bcl-2 also inhibits Aβ-induced neurotoxicity (Cardoso et al., 2001; Morais Cardoso et al., 2002). Interestingly, either PLD3^{WT} or PLD3^{VM} expression in Aβ-fly brains increased Bcl-2 protein levels, which could explain the extended lifespan and climbing abilities of these two genotypes compared with the Aβ-fly control (Fig. 1A and B). However, we also observed that PLD3^{WT} expression significantly reduces the active caspase-3 levels, while PLD3^{VM} expression appeared to be less protective (Fig. 3B). The western blot results for *elav^{c155}-Gal4 > Aβ42^{arc}, dPLD3^{KD}* were virtually indistinguishable from those of the control Aβ flies. We also observed lower Bcl-2 protein levels in oligomeric Aβ-treated SH-SY5Y cells, consistent with the in vivo results, but they returned to the control levels after PLD3^{WT} expression (Fig. S5).

3.4. PLD^{WT} rather than PLD3^{VM} normalizes essential phospholipid levels in Aβ-fly brains

Ethanolamine plasmalogens, especially abundant in the brain (Brites et al., 2004), are essential lipophilic antioxidants (Engelmann, 2004). A liquid chromatography-tandem mass spectrometry (LC-MS/MS) profile of the lipids in methanol extracts of Aβ-fly-brain (Fig. 3C) showed several essential phospholipids, mainly C18 plasmalogens (phosphatidylethanolamine [18:1-PE] and phosphatidylcholine [18:1-PC]) that exhibited a > 1.5-fold increase (Fig. 3C). The increase in antioxidant phospholipids potentially reflects an attempt to counteract the Aβ-induced cell inflammation, oxidative stress, neuronal cell damage, and neurodegeneration as observed in previous publications (Crowther et al., 2005; Iijima et al., 2004). Notably, PLD3^{WT} expression reduced the C18 plasmalogen levels in Aβ-fly brains to the levels found in control fly brains (where all genotypes were under *elav^{c155}-Gal4* driver). Expression of PLD3^{VM} was not sufficient to decrease the antioxidant phospholipid levels and therefore did not reverse the inflammation and neuronal stress. This data confirmed that PLD3^{WT} improves neuronal homeostasis while V232 M leads to an inefficient neuronal defense mechanism.

3.5. V232 M substitution alters a distinct O-glycosylation pattern in PLD3

An initial C-terminal hemagglutinin (HA)-tag detection of PLD3^{WT} and PLD3^{VM} in protein extracts from fruit fly heads (*elav^{c155}-Gal4 > UAS-hPLD3*) revealed that the two variants exhibit a distinct shift in protein molecular weight (Fig. S6). Shifts in PLD3 molecular weight as a result of probable posttranslational modifications were also speculated in previous publications (Munck et al., 2005; Satoh et al., 2014). We also suspected an altered glycosylation pattern in PLD3^{VM} to be the cause of this shift and plausibly an inefficient protein trafficking along the ER-Golgi-endosome axis. In order to study the post-translational modifications of PLD3 and its cellular localization, we expressed variants of the protein in SH-SY5Y cells (Fig. 4A, Methods). Mammalian cell expression system is one of the most suitable choice because the cellular machinery permits correct protein folding and glycosylation patterns similar to those of human cells. Mammalian cell culture can also provide a sufficiently bigger cellular components size; a typical neuron in the head of *D. melanogaster* has a soma diameter of 2–6 μm, compared with 10–30 μm for a pyramidal cell in rodent cortex (Mason and Larkman, 1990). Likewise, in SH-SY5Y cells the slower-migrating upper protein bands (higher molecular weight, HMW) that are well-evident in PLD3^{WT} were less intense in the case of PLD3^{VM} (Fig. 4A, −R, white arrow) and under glycoprotein denaturing conditions, PLD3^{VM} was mainly present as lower molecular weight (LMW) bands (Fig. 4A and E). We assumed that the upper PLD3^{WT} bands represent glycosylated proteins processed through the Golgi apparatus. To examine this hypothesis, we incubated total (PLD3) cell lysates with endoglycosidase H (Endo-H), O-glycosidase (O-Gly) and Peptide-N-glycosidase F (PNGase-F) (Fig. 4A and B). Proteins without signal peptides (i.e. PLD3) might not be exposed to N-linked glycosylation in vivo even though they contain potential motifs, however a single N-glycosylation at the luminal pN132 of hPLD3 (Fig. S1) could not be ruled out. After Endo-H treatment, the recombinant PLD3^{WT} with lower molecular weight shifted to a band of approximately 60 kDa, i.e., Endo-H sensitive (Fig. 4A −S, black arrow). The higher molecule weight PLD3^{WT} protein bands resisted the Endo-H treatment (Fig. 4A, R, white arrowhead and Fig. 4E). In contrast, PLD3^{VM} was Endo-H sensitive, which was also observed in protein extracts from fly heads (*elav^{c155}-Gal4 > UAS-PLD3^{VM}*, Fig. S6). Similar results were seen after PNGase-F treatment (Fig. 4B). With O-glycosidase treatment, however, the upper protein bands in PLD3^{WT} were reduced (Fig. 4B and E) while the PLD3^{VM} pattern was unaffected. We confirmed this glycosylation pattern by treatment with brefeldin A (BFA), an inhibitor of protein transport to the Golgi apparatus. After 2 h of treatment with BFA, the higher molecular weight protein bands were absent (Fig. 4C, white arrowhead). The localization to the Golgi also implies a more complex cellular function than just a robust ER homeostasis.

We predicted three putative O-linked glycosylation sites in hPLD3 between the HKD1 and HKD2 motifs (Munck et al., 2005; Nelson and Frohman, 2015) with positions pS263, pT264, and pT271 (the highest O-glycosylation probability, NetOGlyc 4.0, Fig. S1B). From them, only pT271 was very conserved among the aligned PLD3 peptides (Fig. S1B). To confirm that V232 M variant impairs the O-glycosylation of PLD3, we generated five O-glycosylation-site substitutions in PLD3. Three consecutive and independent transient transfections in SH-SY5Y cells showed that only T271A substitution (PLD3^{T271A}) eliminates the

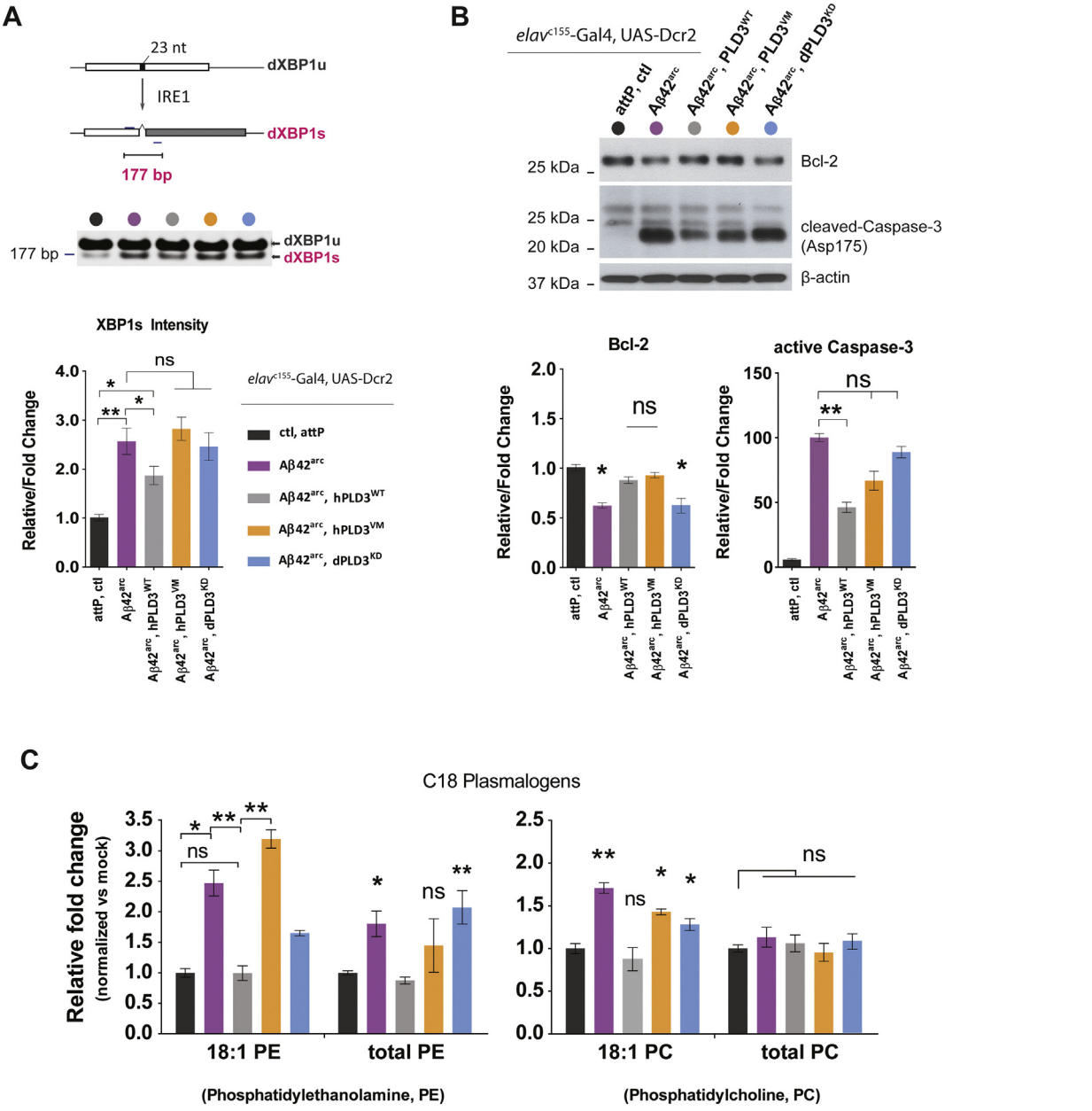

Fig. 3. PLD^{WT} reduces Aβ-induced ER stress, and neuronal apoptosis, and normalizes the phospholipid composition in vivo, while PLD3^{VM} is less effective. (A) Inositol-requiring enzyme 1 (IRE1) mediates alternative *XBP1* splicing in *D. melanogaster* (the scheme is not to scale). Flies expressing Aβ42^{arc} under the control of *elav^{c155}-Gal4* accumulate greater amounts of *XBP1s* (spliced form) than the control flies *elav^{c155}-Gal4 > attP*. Expression of PLD3^{WT} in *elav^{c155}-Gal4 > Aβ42^{arc}* flies rather than PLD3^{VM} or PLD3 knockdown (dPLD3^{KD}) reduces the ER-stress dependent production of *XBP1s*. The colour-coding applies to all panels in the figure. All genotypes were under control of the *elav^{c155}-Gal4* driver (including *UAS-Dcr2*). (B) Protein samples from Aβ42^{arc} fly brains exhibit an increase in active cleaved-caspase 3, indicative of apoptosis, which is reduced significantly after PLD3^{WT} expression. This reduction is not prominent after expression of PLD3^{VM} or dPLD3^{KD} in Aβ flies. However, the anti-apoptotic protein Bcl-2, localizing to the mitochondria, is recovered after the expression of either PLD3^{VM} or PLD3^{WT}. (C) Alterations in anti-oxidative C18 phospholipids in Aβ-flies expressing PLD3^{WT}, PLD3^{VM}, or dPLD3^{KD}. The C18 plasmalogens phosphatidylethanolamine (PE) and phosphatidylcholine (PC) are elevated in methanol extracts of Aβ-fly brains but rescued to normal levels only after expression of PLD3^{WT}. In contrast, PLD3^{VM} expression or dPLD3^{KD} does not regulate these phospholipid levels. We represented all values as mean ± SEM. *, P < 0.05; **, P < 0.01; ***, P < 0.005; One-Way ANOVA with Bonferroni's correction. See also Figs. S2 and S5.

highest HMW protein bands of PLD3, with a protein distribution very similar to that observed for PLD3^{VM}. Further analysis of the glycosylation status of PLD3^{T271A} revealed no shift after O-glycosidase treatment and that the PLD3^{VM} precisely mimics the impaired glycosylation pattern observed in the PLD3^{T271A} variant (Fig. 4E). Thus, V232 M substitution affects the glycosylation of PLD3 and might also alter the protein trafficking and cellular functions.

3.6. *PLD3^{VM} variant affects lysosomal function*

Fazzari et al. recently reported that PLD3 knockout causes enlarged, abnormal lysosomes and colocalization of PLD3 with lysosome-associated membrane protein 1 (LAMP1) (Fazzari et al., 2017). Anomalous PLD3^{VM} trafficking could also affect the lysosomes or the structures and functions of other cellular compartments. Indeed, with Lysotracker-labeled HeLa cells we found enlarged lysosomal structures in cells expressing PLD3^{VM} or PLD3^{T271A} (Fig. 5A) but standard and even reduced

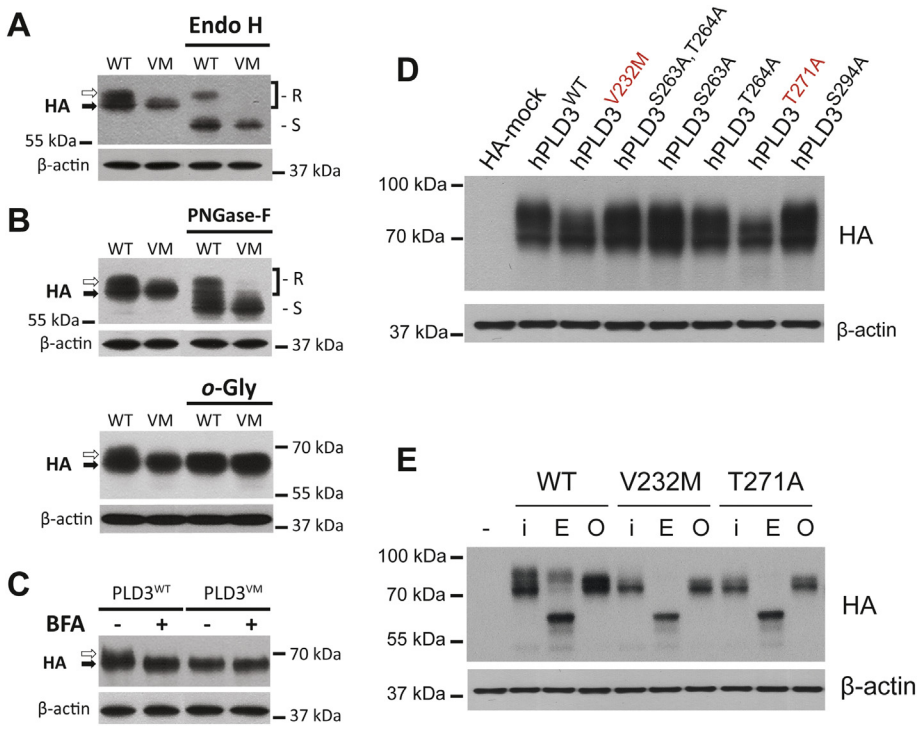

Fig. 4. V232 M substitution alters a distinct O-glycosylation pattern in PLD3.
(A) Protein extracts from SH-SY5Y cells expressing PLD3^{WT} or PLD3^{VM} treated with Endo-H glycosidase; the upper, higher molecular weight (HMW) band (white arrowhead) does not appear in the PLD3^{VM}-expressing cells. The thick, 65-kDa band (black arrowhead) shifts to approximately 50 kDa after Endo-H treatment (S, Endo-H sensitive), identifying this band as PLD3 glycosylated with high-mannose oligosaccharides in the endoplasmic reticulum (ER). The upper, HMW band does not shift after Endo-H treatment (white arrowhead, R, Endo-H resistant). The Endo-H–resistant band is evident in the PLD3^{WT}-expressing cells but not in the PLD3^{VM}-expressing cells. (B) SH-SY5Y cell extracts expressing PLD3^{WT} or PLD3^{VM} treated with brefeldin-A (BFA); the upper, HMW bands of PLD3^{WT} (white arrow) disappear after BFA treatment. (C) We treated protein samples from SH-SY5Y cells expressing PLD3^{WT} or PLD3^{VM} with PNGase-F or O-glycosidase. The upper, HMW band (white arrowhead) does not shift after PNGase treatment but disappears after O-glycosidase treatment. (E) We generated single missense substitutions in four putative O-glycosylation sites between the HKD1 and HKD2 and examined the resulting PLD3 mutants by western blot under glycoprotein-denaturation conditions. Only the T271A substitution resulted in a pattern like that of the PLD3^{VM}. (D) Protein extracts containing PLD3^{WT}, PLD3^{VM} or PLD3^{T271A} treated with Endo-H and O-glycosidase under glycoprotein-denaturation conditions; the Endo-H–resistant protein bands seen in WT are absent in both mutants. O-glycosidase treatment reduces the HMW band size only in extracts containing PLD3^{WT}. I, whole protein extract; E, EndoH-treated extracts; O, O-glycosidase treated extracts. See also Figs. S1 and S6.

lysosomal diameters in cells expressing PLD3^{WT} (Fig. 5B). In vivo, Aβ-fly brains expressing the PLD3^{VM} also exhibited increased LAMP1-positive structures in the Kenyon cells (Fig. S7), while PLD3^{WT} expression led to no significant change in lysosomal structures compared with Aβ-control fly brains. PLD3^{VM} was predominantly distributed as large accumulations that did not completely overlap with the lysosome structures (Fig. S7), implying that these were sizeable insoluble cellular or extracellular PLD3 accumulations. Of note, these accumulated over a period of 20 days in vivo in the AD model flies.

To compare lysosomal constituents and characteristics, we generated iodixanol-gradient fractions from HeLa cells expressing PLD3^{WT}, PLD3^{VM,} and PLD3^{T271A}. LAMP1 exhibited a noticeable shift in earlier fractions (f1–f3) for all samples from the three PLD3 variants. However, PLD3^{VM} and PLD3^{T271A} expression in HeLa cells led to significant retention of LAMP1 in the later fractions (f5–f9) (Fig. 5C, graph) compared with PLD3^{WT} expression. These shifts confirmed that the lysosomes in PLD3^{VM}-expressing cells are denser and produced heavier fractions and, in the case of PLD3^{T271A}, even form more substantial accumulations, with a shift to f7–f9 (Fig. 5C, graph). Interestingly, the total LAMP1 protein exhibited equivalent cellular levels after expression of PLD3^{WT}, PLD3^{VM}, or PLD3^{T271A} (Fig. 5D).

Reduced cathepsin B and L activity correlate with increased Lysotracker-positive compartments and dysfunctional lysosomes (Jung et al., 2015). The active cathepsin B was raised in PLD3^{WT} cells, while cathepsins B and D were significantly reduced in extracts of cells containing PLD3^{VM} and PLD3^{T271A} (Fig. 5D). Interestingly, a knockdown by siRNA targeting the non-coding sequence of the endogenous PLD3 (ncPLD3 siRNA) in HeLa cells also increases the lysosomal diameter (Fig. 6A). The effect was the same in HeLa cells expressing PLD3^{VM} or PLD3^{T271A} with or without ncPLD3 siRNA treatment (Fig. 6C). PLD3 overexpression rescues the phenotype seen in ncPLD3 siRNA treated HeLa cells (Fig. 6C), and Lysotracker puncta appear regular in shape and somewhat smaller in size. Three independent tests showed that the protein levels of the overexpressed PLD3 variants were not affected in the presence of ncPLD3 siRNA (Fig. 6B). Our data is in agreement with previous observations for PLD3 (Fazzari et al., 2017; Palmieri et al., 2011). Altogether, these lysosome findings highlight partial impairment of lysosomal function in the presence of PLD3^{VM} or with knockdown of the endogenous PLD3. However, more complex cellular events, such as aberrant mitochondrial and peroxisomal function, blockage in retrograde trafficking and recycling (Breusegem and Seaman, 2014) and changes in membrane composition could be contributing to the reduced protective function of PLD3^{VM}, we observed in vivo. To confirm differences in the PLD3 variants membrane localization, we performed a fluorescence-activated cell sorting (FACS) analysis of cells expressing three PLD3 variants, immunolabeled without cell permeabilization (Fig. 6D). This experiment revealed that membrane localization of PLD3^{VM} and PLD3^{T271A} was significantly reduced compared with PLD3^{WT} under the same experimental conditions, which suggest a blockage in ER-Golgi-to-membrane transport. We assumed that PLD3 trafficking to the membrane is not efficient in the case of the V232 M and T271A variants due to reduced O-linked glycosylation in the Golgi.

4. Discussion

Glycosylation is essential in protein trafficking, localization, and cellular function. An impaired glycosylation pattern was recently found to affect the regular traffic and function of triggering receptor expressed on myeloid cells 2 (TREM2), thus increasing the risk of AD (Kleinberger et al., 2014; Park et al., 2015; Park et al., 2016). Similarly, impaired glycosylation in PLD3^{VM} (Fig. 4) could explain the diminished protective effect observed in vivo (Fig. 1). Out of three putative O-glycosylation sites (Fig. S1), only T271A substitution in PLD3 exhibits a reduction of the higher molecular weight bands (Fig. 4D). Under glycoprotein-denaturing conditions, the PLD3^{VM} variant reproduced the PLD3^{T271A} distribution which marks a lack of putative O-glycosylation site. O-linked glycosylation of PLD3 also appears to impact an efficient membrane localization as judged by the FACS data from the three PLD3 variants (Fig. 6D), where PLD3^{VM} again showed similarity with the PLD3^{T271A} rather than PLD3^{WT}.

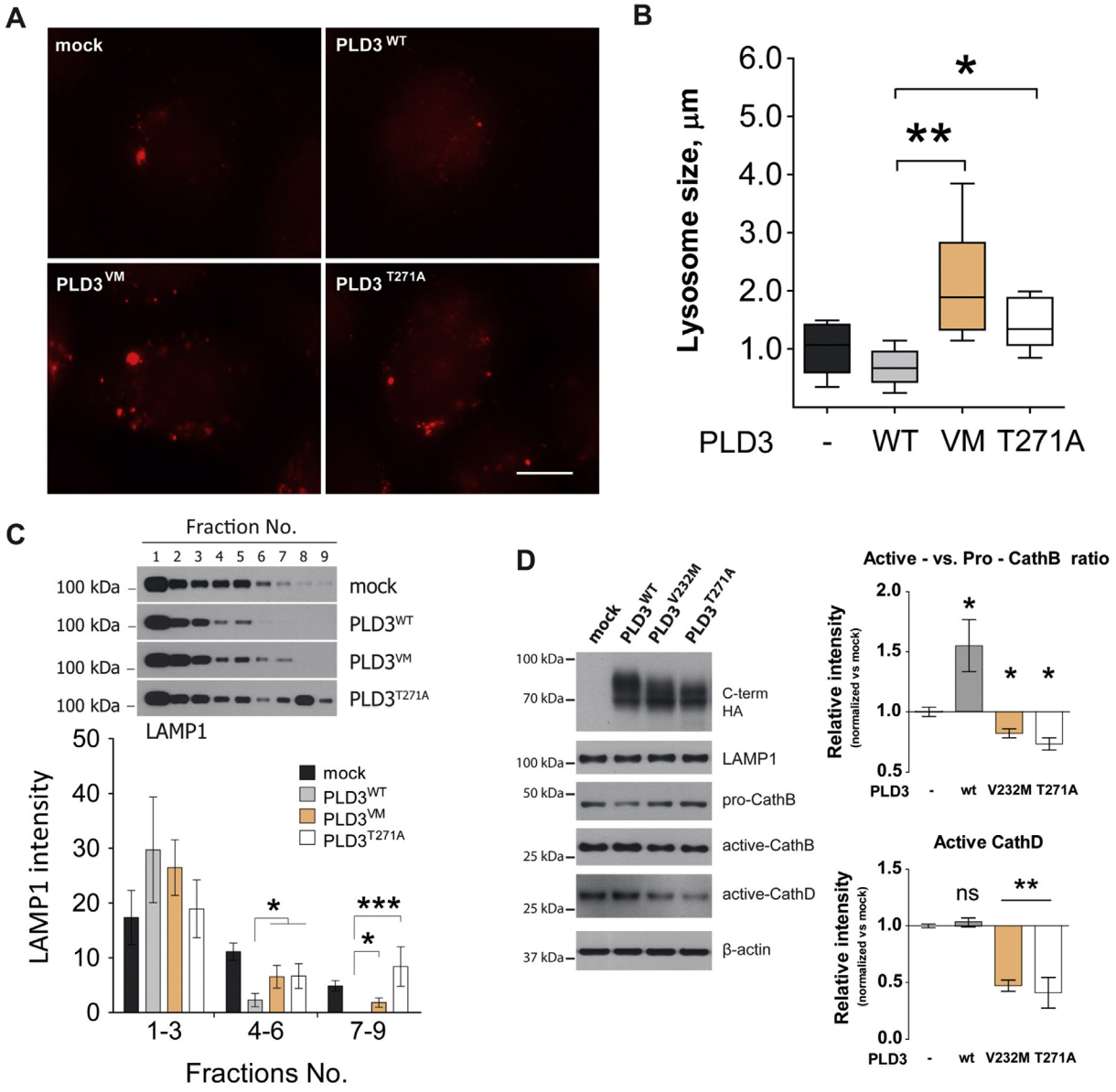

Fig. 5. PLD3^{VM} variant affects the lysosomal function.
(A) Lysotracker staining (red) in HeLa cells (expressing PLD3^{WT}, PLD3^{VM}, or PLD3^{T271A}). We observed increased lysosome size (diameter) after expression of PLD3^{VM} or PLD3^{T271A}. (B) Quantification of the lysosome structures for the genotypes described in (A). The images in (A) and the quantifications in (B) are from high-content imaging data (see materials and methods). (C) iodixanol-gradient fractionation from HeLa cells expressing PLD3^{WT}, PLD3^{VM}, or PLD3^{T271A}. To quantify the differences in fractions, we binned each fraction into 3 groups: f1–3, f4–6, and f7–8 (bottom graph). After PLD3^{WT} expression, LAMP1-positive fractions were observed mainly in f1 to f3. Heavier and denser lysosomal structures may fuse with other cellular compartments, causing the LAMP1 to shift into f5-f8, as we observed in PLD3^{VM}, or PLD3^{T271A} expressing cells. (D) Western blot analysis of the same genotypes for essential lysosomal markers. The active cathepsin B and D (CathB and CathD) proteases show a significant reduction in HeLa cells expressing PLD3^{VM}, or PLD3^{T271A} while PLD3^{WT} expression statistically increased the CathB activity. The total cell extracts do not show significant variation for the lysosome marker, LAMP1. We represented all values as mean ± SEM. *, $P < 0.05$; **, $P < 0.01$; ***, $P < 0.005$; One-Way ANOVA with Bonferroni's correction. Scale bar: 20 µm. (For interpretation of the references to colour in this figure legend, the reader is referred to the web version of this article.)

In earlier studies, PLD3 showed immunoreactivity within the ER (Munck et al., 2005; Osisami et al., 2012), whereas later studies revealed a multi-compartmentalization with partial overlap with the lysosomes and the endosomes (Fazzari et al., 2017; Mukadam et al., 2018). Fazzari et al. recently reported that PLD3 deficiency leads to defects in lysosomal structures (Fazzari et al., 2017). In the brains of PLD3 knockout mice, lysosomes are enlarged and dented and may contain explicit inclusions resembling lipid droplets, implying that PLD3 might be necessary for the typical structure and function of lysosomes and neuronal lipid metabolism. Our data showed that PLD3 knockdown also produces enlarged Lysotracker-positive compartments (Fig. 6A). Although PLD3 may not be essential for cell survival (Fazzari et al., 2017), our data imply that PLD3^{WT} expression enhances subcellular compartments, localization and function, which may not be as precise in the presence of PLD3^{VM} or PLD3^{T271A}. Expression of PLD3^{VM} and PLD3^{T271A} in HeLa cells also showed remarkably clustered lysosomes (Fig. 5). Compared with PLD3^{WT}-transfected cells, the LAMP1 distribution shifted toward the heavier fractions in cells expressing PLD3^{VM} or PLD3^{T271A} (Fig. 5). This shift in the iodixanol-gradient fractions may also reflect alterations in lysosomal constituents and characteristics. V232 M and T271A substitutions in hPLD3 still produced enlarged lysotracker inclusions in HeLa cells where endogenous

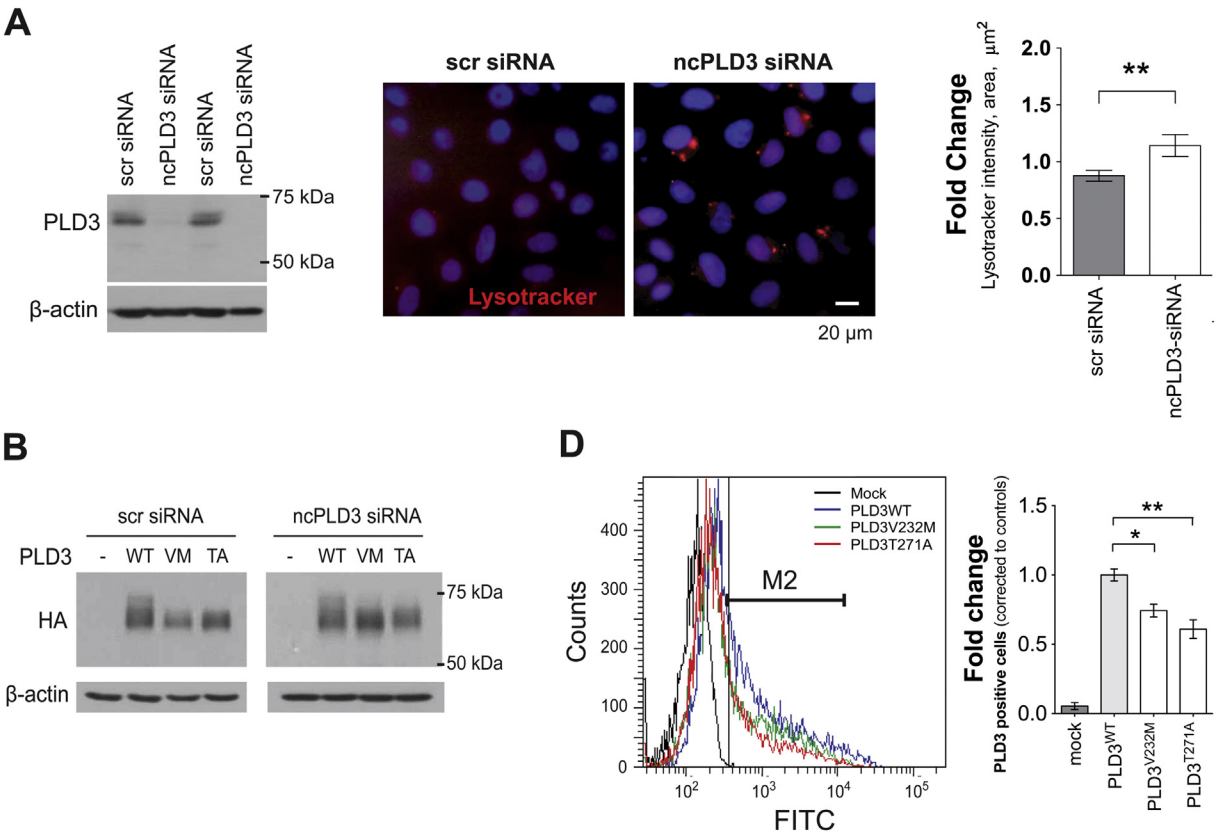

(caption on next page)

Fig. 6. Lysosome dynamics in HeLa cells overexpressing PLD3 variants and after knockdown of the endogenous PLD3. (A) HeLa cells treated with non-coding siRNA of PLD3 (ncPLD3 siRNA, the Western analysis in the middle) shows a specific reduction of the endogenous PLD3 compared with cells treated with scrambled siRNA (scr siRNA). We should note that the detection of endogenous PLD3 produced a weak signal in HeLa cells. Immunostaining with Lysotracker shows increased puncta in ncPLD3 siRNA treated HeLa cells (A, the image on the right). The estimated immunofluorescence area of lysotracker puncta per cell (red) within the HeLa cells treated with non-coding siRNA (ncPLD3 siRNA, 14 cells) revealed increased lysosome size (mm^2) (A, graph on the left) compared with the control scrambled scr siRNA-treated cells (16 cells); (B) Western blot analysis of non-coding siRNA transfected HeLa cells, transiently expressing PLD3 variants shows no reduction of the overexpressed PLD3 variants; the endogenous PLD3 was knockdown with siRNA targeting three independent introns in PLD3 precursor-mRNA; (C) Under the same conditions as in (B) lysotracker (red) shows the lysosomal compartments in HeLa cells. Lysotracker accumulates in the lysosomal compartments of HeLa cells expressing $PLD3^{VM}$, or $dPLD3^{T271A}$, with or without knockdown of the endogenous PLD3. $PLD3^{WT}$ rescued this phenotype and as seen from the quantification on the right even showed slightly but not significantly reduced lysosome volume; (D) Membrane localization of three PLD3 variants in fluorescence-activated cell sorting (FACS) analysis. The histogram represents the results from three independent transfections with each of the three PLD3 variants tested. We labeled the HeLa cell membrane by HA antibody (for PLD3 variants) under non-denaturation conditions, followed by FITC-conjugated goat-anti-rat secondary antibodies. The graph on the right represents the percent of cells with fluorescence intensity compared with a reading of nonspecific fluorescence (mock). Marker M2 is placed to the right of the control cutoff value to designate positive events. Both variants V232 M and T271A showed decreased membrane localization compared with the surface-bound PLD^{WT}. All values are the mean ± SEM. *, $P < 0.05$; **, $P < 0.01$; One-Way ANOVA with Bonferroni's correction. Scale bar, 20 μm. (For interpretation of the references to colour in this figure legend, the reader is referred to the web version of this article.)

pld3 was targeted with non-coding siRNA (Fig. 6C). Therefore, O-glycosylation of PLD3 is not only essential for Golgi-lysosomal trafficking and the lysosome structure and function but a more central cellular sorting compartments could also be affected by the presence of the WT and V232 M variants of PLD3.

$PLD3^{WT}$ expression significantly extended the lifespan and alleviated Aβ-induced memory loss and neurodegenerative behavior (Figs. 1, 2, and 3). We observed reduced neuroprotective activity in Aβ-flies expressing $PLD3^{VM}$ (Figs. 1, 2, and 3), suggesting that the V232 M has real biological effects on AD pathogenesis. $PLD3^{VM}$ variant did not augment further the Aβ-induced neurodegenerative symptoms (Fig. 1A and B) but, compared with $PLD3^{WT}$, did not produce sufficiently positive effect either. Thus, V232 M could be a loss-of-protective-function substitution rather than a gain-of-toxic-function mutation. Knockdown of endogenous PLD3 aggravated the neurodegenerative behavior and attenuated the Aβ-flies longevity (Figs. 1 and 2). Ubiquitous expression of dPLD3-RNAi by $elav^{c155}$-*Gal4* could produce quick aggravation of the Aβ-fly behavior and lifespan (Fig. 1), but our observation for the intensity of FasII in the MBs differed from Aβ-flies control (Fig. 2). First, the flies ($elav^{c155}$-*Gal4* > $Aβ42^{arc}$, $dPLD3^{KD}$) used in the immunohistochemistry were 20 days old, and their survival was already significantly reduced. We could speculate that some of the RNAi-expressing animals did not knockdown or express $Aβ^{arc}$ as well as others who died at a younger age. In other words, attrition could have enriched the fly cohort in animals that had not knocked down well, skewing the following results and exhibiting less aggravation of the FasII intensity. Second, the climbing assay reflects the fact that $elav^{c155}$-*Gal4* driver strongly expresses in fly CNS including the motor neurons, while the mushroom bodies show only a specific portion of the brain. Moreover, we found no promoter competition as Aβ mRNA levels were comparable in all tested genotypes (Fig. S2C), which validates the in vivo effects we observed after overexpression of PLD3 variants in Aβ-flies.

An abnormal protein folding could lead to altered protein glycosylation and Golgi trafficking but also protein aggregation, as we observed in fly brains expressing $PLD3^{VM}$ (Fig. S7). The PLD3 mutants' lack of interaction with other vital neurodegeneration-related molecules such as granulin (Satoh et al., 2014), and phospholipase A2 (Davids et al., 2016) could enhance cell degeneration in the presence of amyloid accumulations through induction of Golgi abnormalities. This hypothesis could be an attractive target for further investigation.

Author's contributions

Methodology, AVD, and SYY; Writing – original draft, AVD, and SYY; Investigation, AVD, HLS, MHC, JJP, HJY, and KMC; Review and editing, AVD, HLS, DHK, and SYY; AVD and HLS contributed equally to this work.

Funding disclosure

This study was supported by Basic Science Research Program through the National Research Foundation of Korea(NRF) funded by the Ministry of Science, ICT and future Planning [grant nos. 2018R1A2A1A05077403 and 2017R1A2B2010901].

Potential conflict of interests

The authors declare no competing interests.

Appendix A. Supplementary data

Supplementary data to this article can be found online at https://doi.org/10.1016/j.nbd.2019.05.015.

References

Bier, E., 2005. Drosophila, the golden bug, emerges as a tool for human genetics. Nat. Rev. Genet. 6, 9–23.
Breusegem, Sophia Y., Seaman, Matthew N., 2014. Genome-wide RNAi screen reveals a role for multipass membrane proteins in endosome-to-Golgi retrieval. Cell Rep. 9, 1931–1945.
Brites, P., et al., 2004. Functions and biosynthesis of plasmalogens in health and disease. Biochim. Biophys. Acta 1636, 219–231.
Brunner, Y., et al., 2007. Proteomics analysis of insulin secretory granules. Mol. Cell. Proteomics 6, 1007–1017.
Cai, D., et al., 2006a. Phospholipase D1 corrects impaired betaAPP trafficking and neurite outgrowth in familial Alzheimer's disease-linked presenilin-1 mutant neurons. Proc. Natl. Acad. Sci. U. S. A. 103, 1936–1940.
Cai, D., et al., 2006b. Phospholipase D1 corrects impaired βAPP trafficking and neurite outgrowth in familial Alzheimer's disease-linked presenilin-1 mutant neurons. In: Proceedings of the National Academy of Sciences of the United States of America. vol. 103. pp. 1936–1940.
Cardoso, S.M., et al., 2001. Functional mitochondria are required for amyloid beta-mediated neurotoxicity. FASEB J. 15, 1439–1441.
Casas-Tinto, S., et al., 2011. The ER stress factor XBP1s prevents amyloid-beta neurotoxicity. Hum. Mol. Genet. 20, 2144–2160.
Crittenden, J.R., et al., 1998. Tripartite mushroom body architecture revealed by antigenic markers. Learn. Mem. 5, 38–51.
Crowther, D.C., et al., 2005. Intraneuronal Abeta, non-amyloid aggregates and neurodegeneration in a Drosophila model of Alzheimer's disease. Neuroscience 132, 123–135.
Cruchaga, C., et al., 2014. Rare coding variants in the phospholipase D3 gene confer risk for Alzheimer's disease. Nature 505, 550–554.
Davids, M., et al., 2016. Disruption of Golgi morphology and altered protein glycosylation in PLA2G6-associated neurodegeneration. J. Med. Genet. 53, 180–189.
Davis, R.L., Han, K.-A., 1996. Neuroanatomy: mushrooming mushroom bodies. Curr. Biol. 6, 146–148.
Dietzl, G., et al., 2007. A genome-wide transgenic RNAi library for conditional gene inactivation in Drosophila. Nature 448, 151–156.
Engelmann, B., 2004. Plasmalogens: targets for oxidants and major lipophilic antioxidants. Biochem. Soc. Trans. 32, 147–150.
Fazzari, P., et al., 2017. PLD3 gene and processing of APP. Nature 541, E1–E2.
Ferreiro, E., et al., 2007. Bcl-2 overexpression protects against amyloid-beta and prion toxicity in GT1-7 neural cells. J. Alzheimers Dis. 12, 223–228.
Freeman, M., 1996. Reiterative use of the EGF receptor triggers differentiation of all cell types in the Drosophila eye. Cell 87, 651–660.
Hawrylycz, M.J., et al., 2012. An anatomically comprehensive atlas of the adult human

brain transcriptome. Nature 489, 391–399.
Heilmann, S., et al., 2015. PLD3 in non-familial Alzheimer's disease. Nature 520, E3–E5.
Hockenbery, D.M., 1995. Bcl-2, a novel regulator of cell death. Bioessays 17, 631–638.
Hooli, B.V., et al., 2015. PLD3 gene variants and Alzheimer's disease. Nature 520, E7–E8.
Iijima, K., et al., 2004. Dissecting the pathological effects of human Abeta40 and Abeta42 in Drosophila: a potential model for Alzheimer's disease. Proc. Natl. Acad. Sci. U. S. A. 101, 6623–6628.
Jung, M., et al., 2015. Cathepsin inhibition-induced lysosomal dysfunction enhances pancreatic Beta-cell apoptosis in high glucose. PLoS ONE 10, e0116972.
Karch, C.M., Goate, A.M., 2015. Alzheimer's disease risk genes and mechanisms of disease pathogenesis. Biol. Psychiatry 77, 43–51.
Kaun, K.R., et al., 2011. A Drosophila model for alcohol reward. Nat. Neurosci. 14, 612–619.
Kleinberger, G., et al., 2014. TREM2 mutations implicated in neurodegeneration impair cell surface transport and phagocytosis. Sci. Transl. Med. 6, 243ra86.
Kong, W., et al., 2009. Independent component analysis of Alzheimer's DNA microarray gene expression data. Mol. Neurodegener. 4, 5.
Lambert, J.C., et al., 2015. PLD3 and sporadic Alzheimer's disease risk. Nature 520, E1.
Lein, E.S., et al., 2007. Genome-wide atlas of gene expression in the adult mouse brain. Nature 445, 168–176.
Lin, D.M., Goodman, C.S., 1994. Ectopic and increased expression of Fasciclin II alters motoneuron growth cone guidance. Neuron 13, 507–523.
Lin, J.Y., et al., 2014. Intraneuronal accumulation of Abeta42 induces age-dependent slowing of neuronal transmission in Drosophila. Neurosci. Bull. 30, 185–190.
Mason, A., Larkman, A., 1990. Correlations between morphology and electrophysiology of pyramidal neurons in slices of rat visual cortex. II. Electrophysiology. J. Neurosci. 10, 1415–1428.
Morais Cardoso, S., et al., 2002. Induction of cytochrome c-mediated apoptosis by amyloid beta 25-35 requires functional mitochondria. Brain Res. 931, 117–125.
Mukadam, A.S., et al., 2018. Analysis of novel endosome-to-Golgi retrieval genes reveals a role for PLD3 in regulating endosomal protein sorting and amyloid precursor protein processing. Cell. Mol. Life Sci. 75 (14), 2613–2625.
Munck, A., et al., 2005. Hu-K4 is a ubiquitously expressed type 2 transmembrane protein associated with the endoplasmic reticulum. FEBS J. 272, 1718–1726.
Nelson, R.K., Frohman, M.A., 2015. Physiological and pathophysiological roles for phospholipase D. J. Lipid Res. 56, 2229–2237.
Oliveira, T.G., et al., 2010. Phospholipase D2 ablation ameliorates Alzheimer's disease-linked synaptic dysfunction and cognitive deficits. J. Neurosci. 30, 16419–16428.
Ollmann, M., et al., 2000. Drosophila p53 is a structural and functional homolog of the tumor suppressor p53. Cell 101, 91–101.
Osisami, M., et al., 2012. A role for phospholipase D3 in myotube formation. PLoS ONE 7, e33341.
Packard, M., et al., 2003. FASt remodeling of synapses in Drosophila. Curr. Opin. Neurobiol. 13, 527–534.
Palmieri, M., et al., 2011. Characterization of the clear network reveals an integrated control of cellular clearance pathways. Hum. Mol. Genet. 20, 3852–3866.
Park, J.S., et al., 2015. Disease-associated mutations of TREM2 Alter the processing of N-linked oligosaccharides in the Golgi apparatus. Traffic 16, 510–518.
Park, J.S., et al., 2016. The Alzheimer's disease-associated R47H variant of TREM2 has an altered glycosylation pattern and protein stability. Front. Neurosci. 10, 618.
Pech, U., et al., 2013. Mushroom body miscellanea: transgenic Drosophila strains expressing anatomical and physiological sensor proteins in Kenyon cells. Front. Neural Cir. 7, 147.
Pedersen, K.M., et al., 1998. Expression of a novel murine phospholipase D homolog coincides with late neuronal development in the forebrain. J. Biol. Chem. 273, 31494–31504.
Porter, A.G., Janicke, R.U., 1999. Emerging roles of caspase-3 in apoptosis. Cell Death Differ. 6, 99–104.
Satoh, J.-i., et al., 2014. PLD3 is accumulated on neuritic plaques in Alzheimer's disease brains. Alzheimers Res. Ther. 6 (70–70).
Tennessen, J.M., et al., 2014. Methods for studying metabolism in Drosophila. Methods 68, 105–115.
Xu, P.-T., et al., 2006. Differences in apolipoprotein E3/3 and E4/4 allele-specific gene expression in hippocampus in Alzheimer disease. Neurobiol. Dis. 21, 256–275.
Yoshida, H., et al., 2001. XBP1 mRNA is induced by ATF6 and spliced by IRE1 in response to ER stress to produce a highly active transcription factor. Cell 107, 881–891.
Zeng, X., et al., 2015. Genome-wide RNAi screen identifies networks involved in intestinal stem cell regulation in Drosophila. Cell Rep. 10, 1226–1238.
Zhang, D.F., et al., 2016. PLD3 in Alzheimer's disease: a modest effect as revealed by updated association and expression analyses. Mol. Neurobiol. 53, 4034–4045.
Zhao, X.L., et al., 2010. Expression of beta-amyloid induced age-dependent presynaptic and axonal changes in Drosophila. J. Neurosci. 30, 1512–1522.
Zheng, L., et al., 2004. An efficient one-step site-directed and site-saturation mutagenesis protocol. Nucleic Acids Res. 32 (e115-e115).